**Author Manuscript**

**Published in final edited form as:**

Biomech Model Mechanobiol. 2017 Apr;16(2):651-666.

Doi: 10.1007/s10237-016-0843-9.

**Title:**

# A mathematical model of tissue-engineered cartilage development under cyclic compressive loading

Cátia Bandeiras and António Completo

Department of Mechanical Engineering, University of Aveiro, Aveiro, Portugal

**Abstract:**

In this work a coupled model of solute transport and uptake, cell proliferation, extracellular matrix synthesis and remodeling of mechanical properties accounting for the impact of mechanical loading is presented as an advancement of a previously validated coupled model for free-swelling tissue-engineered cartilage cultures. Tissue-engineering con- structs were modeled as biphasic with a linear elastic solid, and relevant intrinsic mechanical stimuli in the constructs were determined by numerical simulation for use as inputs of the coupled model. The mechanical dependent formulations were derived from a calibration and parametrization dataset and validated by comparison of normalized ratios of cell counts, total glycosaminoglycans and collagen after 24h continuous cyclic unconfined compression from another dataset. The model successfully fit the calibration dataset and predicted the results from the validation dataset with good agreement, with average relative errors up to 3.1 and 4.3%, respectively. Temporal and spatial patterns determined for other model outputs were consistent with reported studies. The results suggest that the model describes the interaction between the simultaneous factors involved in in vitro tissue-engineered cartilage culture under dynamic loading. This approach could also be attractive for optimization of culture protocols, namely through the application to longer culture times and other types of mechanical stimuli.

Keywords: Tissue-engineered cartilage · Mathematical modeling · Cyclic unconfined compression · Intrinsic mechanical parameters · Cartilage growth

## 1 Introduction

The major challenge associated with tissue-engineered cartilage is the difficulty to approximate the mechanical properties of the new tissues to the native ones. When implanted, these inferior tissues are detrimental due to cell damage and degradation of extracellular matrix (ECM) (Hung et al. 2004; Khoshgoftar et al. 2013; Bandeiras and Completo 2013, 2015). In order to increase the production of extracelular matrix and mechanical properties of the cultured tissues, mechanical stimulation in bioreactors has provided good results. Various experimental studies in bioreactors have shown that the application of cyclic unconfined compression at moderate strains (2–15%) and frequencies (0.01–3Hz) stimulates the production of collagen and proteoglycans and increases the mechanical properties of the constructs (Lee and Bader 1997; Hung et al. 2004; Kisiday et al. 2004; Tsuang et al. 2008; Lin et al. 2014). Computational modeling techniques are useful to establish protocols for mechanical stimulationof tissue-engineered cartilage, as well as to provide further insights on outputs not easily measurable experimentally. Regarding the comparison of multiple amplitudes and frequencies of unconfined compression, reported inferences from numerical approaches are related to the determination of the range of average values of intrinsic mechanical parameters for increased ECM synthesis (Tasci et al. 2011) and gene expression (Wimmer et al. 2003), as well as to the transport and synthesis of solutes and ECM molecules (Gardiner et al. 2007; Evans and Quinn 2006; Sengers et al. 2004a). A validated model that includes the simultaneous modeling of solute transport, cell proliferation, ECM distribution and remodeling of the mechanical proper- ties was proposed and validated for free-swelling cultures with different scaffold geometries (Bandeiras et al. 2015). This modeling approach was also applied and expanded to simulate the short-term impact on construct properties under compression, bending, shear (Bandeiras et al. 2014a) and

hydrostatic pressure (Bandeiras et al. 2014b). The goal of this work is to provide a validated model to study the impact of different sets of amplitudes and fre- quencies for cyclic uniaxial compression stimulation regimes on tissue-engineered cartilage. The numerical outcomes of biochemical entities and remodeling of biphasic mechanical properties will be presented, as well as the intrinsic mechanical parameters that influence the dynamics of these outcomes. For this purpose, a finite element model based on a biphasic constitutive model accounting for remodel- ing of the mechanical properties with the concentration of ECM components will be used. Model calibration will be per- formed first on a dataset with bovine articular chondrocytes seeded in agarose 3% w/w scaffolds loaded at a compres- sive amplitude of 15% of the height at different compressive frequencies (Lee and Bader 1997), and the derived mod- els will be parametrized for a dataset with rat chondrocytes subjected to different compressive frequencies as well at a 15% amplitude (Tsuang et al. 2008). Model validation will be performed by comparing the parametrized model with the results for the several loading conditions at 5 and 10% maximum compressive amplitudes from the same study in terms of cell density, total GAG and collagen synthesis (Tsuang et al. 2008).

## 2 Methods

### 2.1 Governing equations

The construct is modeled in contact with a fluid solution with neutral solutes dissolved. The growing tissue-engineered cartilage is a tissue with two phases: an inviscid and incom- pressible fluid and a compressible elastic solid matrix. The mechanical behavior of the tissue is described by a linear biphasic mixture model (Zhang and Szeri 2005; Sengers et al. 2004b; Mow et al. 1980; Lelli et al. 2015).

### 2.1.1 Conservation of linear momentum

Under the assumption that inertia and body forces are neg- ligible, the total linear momentum balance in the mixture is given by:

$$\nabla\sigma = 0 \tag{1}$$

In the equation above, σ is the total Cauchy stress tensor. The total stress in the mixture accounting for a solid phases and a fluid phase f is given by:

$$\sigma = \sigma^{s} + \sigma^{f} = \sigma^{e} - pI, \tag{2}$$

with $\sigma^e$ the effective stress tensor for the solid matrix, p the pore pressure and I the identity tensor.

### 2.1.2 Conservation of mass

The mass balances for each phase α is:

$$\frac{\partial n^{\alpha}\rho^{\alpha}}{\partial t} + \nabla(n^{\alpha}\rho^{\alpha}v^{\alpha}) = 0, \tag{3}$$

where $n^\alpha$ is the volume fraction of the phase, $\rho^\alpha$ is the intrinsic mass density of the phase, and $v^\alpha$ is the velocity of the phase. The solid phase, $n^s$, is comprised by the agarose matrix volume fraction and grows over time with the increase of cells, collagen and bound glycosaminoglycans (GAGs):

$$n^{s} = n^{\text{agarose}} + n^{\text{cell}} + n^{\text{GAG}_b} + n^{\text{COL}} \tag{4}$$

The solutes dissolved in the fluid volume fraction, $n^f$, have negligible volume, and their mass balance is described by:

$$\frac{\partial n^{f} M^{\beta} c^{\beta}}{\partial t} + \nabla(n^{f} M^{\beta} c^{\beta} v^{f}) = M^{\beta} q^{\beta}, \tag{5}$$

with $M^\beta$ the molar mass of solute β, $c^\beta$ the molar concentration of the solute and $q^\beta$ a source or sink term for the solute that can be created or eliminated, generally depending on the concentrations of other solutes. The total mass balance for the mixture is derived

from the summation of (3) for the solid and fluid phase. The fluid is assumed incompressible, while the solid is compressible. It is also assumed that the solid is completely saturated, meaning that all voids are filled with fluid ($n^s + n^f = 1$).

### 2.1.3 Biphasic model

The effective stress tensor in (2) is described by a linear elastic relationship, assuming that the solid matrix is not intrinsically viscous.

$$\sigma^e = \mathbb{C} : \epsilon \tag{6}$$

In (6), the solid matrix was considered to be initially homogeneous and isotropic, with C as the fourth-order stiffness tensor and $\epsilon$ as the strain tensor. Fluid flow is governed by the Darcy's law, which states that fluid velocity, $v^f$ ($ms^{-1}$), relative to the solid matrix, $v^s$, is proportional to the gradient of the pore pressure $\nabla p$ (Pa) and controlled by the hydraulic permeability, k ($m^4N^{-1}s^{-1}$), of the porous scaffold, accounting as well for the porosity, n, of the material (Sengers et al. 2004b).

$$n(v^f - v^s) = -k\nabla p \tag{7}$$

The permeability was assumed to be initially homogeneous and isotropic. The permeability dependency on the solid ($n^s$) and fluid ($n^f$) volume fractions relatively to a reference permeability ($k_p$) has been implemented following the Carman–Kozeny relationship, which has already been doc- umented to predict the decrease in permeability related to growing biomass in a bioreactor culture of engineered cartilage (Chung et al. 2007; Sacco et al. 2011).

$$k = k_p \frac{(n^f)^3}{(n^s)^2} \tag{8}$$

In order to calculate the porosity of the construct, which is equivalent to the fluid volume fraction under the assumption that the construct is fully saturated with water, the following relationship between porosity and the void ratio, e, of the construct was applied.

The void ratio represents the fraction of void volume ($V_V$) relatively to the total volume ($V_T$) of the construct.

$$e = \frac{V_V}{V_T} \tag{9}$$

### 2.1.4 Nutrient transport and uptake

The transport of nutrients in the constructs is governed by the reaction–advection–diffusion equation with the reactive term described by metabolite uptake to the cells or production by the cells by the Michaelis–Menten kinetics (Sengers et al. 2005; Chung et al. 2007; Nava et al. 2013).

$$\frac{\partial c}{\partial t} - D_{\text{tissue}} \frac{\partial^2 c}{\partial x^2} + v^f \frac{\partial c}{\partial x} = q_{\text{glc}} \tag{10}$$

$$q_{\text{glc}} = -\rho_{\text{cell}} \frac{V_{\max} c}{K_m + c} \tag{11}$$

In the equations above, c represents the concentration of the nutrient (mol $m^{-3}$ ), $D_{tissue}$ the diffusion coefficient of the nutrient in the tissue ( $m^2s^{-1}$ ), $q_{glc}$ the flux of glucose consumption (mol $m^{-3}s^{-1}$), $\rho_{cell}$ the cell density (cells $m^{-3}$),the maximum uptake rate (mol $cell^{-1}s^{-1}$)) and $K_m$ the half maximum rate concentration (mol $m^{-3}$). The diffusion coefficient in the tissue is a fraction of the diffusion coefficient of the solute in water and updated using the Mackie–Mears relationship (Zhang and Szeri 2005).

$$D_{\text{tissue}} = D_{\text{water}} \frac{(n^f)^2}{(2 - n^f)^2} \tag{12}$$

It is considered that glucose metabolism by chondrocytes is approximately anaerobic. Therefore, one mole of glucose consumed leads to the production of two moles of lactate. This relationship is taken into account in the lactate production flux, $q_{lac}$, as follows (Sengers et al. 2005; Hossain et al. 2015):

$$q_{\text{lac}} = -2 * q_{\text{glc}} \tag{13}$$

### 2.1.5 Cell growth

Cell densityis modifiedbymigration, proliferationanddeath. These three mechanisms are governed by the following equation (Galban and Locke 1999; Chung et al. 2006, 2007; Sacco et al. 2011; Nava et al. 2013):

$$\frac{\partial \rho_{\text{cell}}}{\partial t} - D_{\text{cell}} \frac{\partial^2 \rho_{\text{cell}}}{\partial x^2} = (R_{\text{prol}} - R_{\text{death}}) \rho_{\text{cell}} \tag{14}$$

A diffusion coefficient, $D_{cell}$, is introduced due to the assumption that new chondrocytes have mobility due to random walks (Chung et al. 2006). While the death rate per cell, $R_{death}$ (s−1cell−1), is assumed constant, the proliferation rate, $R_{prol}$, is modulated by both metabolic and mechanical factors that decrease the actual proliferation from the maximum proliferation rate, $\mu_{max}$:

$$R_{\text{prol}} = R_{\text{prol,met}} R_{\text{prol,mech}} \mu_{\text{max}} \tag{15}$$

The metabolic ratio, $R_{prol,met}$, is dominated by Monod kinetics on growth stimulation by glucose availability and inhibition by excess lactate concentrations (Hossain et al. 2015). This parameter has values between 0 and 1, given that the decrease in glucose concentrations and the accumulation of lactate has a deleterious effect in proliferation:

$$R_{\text{prol,met}} = \frac{c_{\text{glc}}}{K_{\text{glc}} + c_{\text{glc}}} \left(1 + \frac{c_{\text{lac}}}{K_{\text{lac}}}\right)^{-1} \tag{16}$$

In the equation above, $K_{glc}$ and $K_{lac}$ represent the half- rate concentration for glucose and lactate, respectively. The mechanical ratio, $R_{prol,mech}$, accounts for two opposite effects: a positive effect of shear stress in proliferation, described by a linear relationship with shear stress rate $\tau_{shear} * f$ (Pa), and a negative effect of excessive compressive strain through the minimum principal strain $\epsilon_{min,prin}$ (Lee and Bader 1997). This mechanical modulation factor hence takes values larger or equal to zero. The shear stress equation was adapted from a validated equation for perfusion stimuli accounting for an increase in the value of the proliferation rate with the increase in the applied shear stress (Sacco et al. 2011; Hossain et al. 2015).

$$R_{\text{prol,mech}} = 1 - \alpha * \epsilon_{\text{min,prin}} + \beta * \tau_{\text{shear}} f \tag{17}$$

### 2.1.6 ECM growth

We assume that the synthesized glycosaminoglycans (GAGs) are distributed into two fractions: an unbound one, released to the culture media ($GAG_{ub}$), and a bound one ($GAG_b$) that forms ECM with the collagen fibers (Wilson et al. 2002; Nikolaev et al. 2010; Haider et al. 2011). It is assumed that, upon synthesis, all GAGs are released and are then bound to the matrix according to a first-order binding kinetics. It is also considered that GAG synthesis saturates at a given equilibrium concentration:

$$\begin{aligned}\frac{\partial \text{GAG}_{\text{ub}}}{\partial t} - D_{\text{GAG}} \frac{\partial^2 \text{GAG}_{\text{ub}}}{\partial x^2} + v^{\text{f}} \frac{\partial \text{GAG}_{\text{ub}}}{\partial x} \\ = k_{\text{GAG},s} \rho_{\text{cell}} (\text{GAG}_{b,\text{ss}} - \text{GAG}_b) - k_{\text{GAG},b} \text{GAG}_{\text{ub}}\end{aligned} \tag{18}$$

$$\frac{\partial \text{GAG}_b}{\partial t} = k_{\text{GAG},b} \text{GAG}_{\text{ub}} \tag{19}$$

Since GAGs are fundamental to the compressive resistance of cartilage, we assume that the synthesis is modulated by the compressive strain and its rate. There is experimental evidence that GAG synthesis is optimal at a given cell volume, below and above which the synthesis rate starts to decay (Gao et al. 2015) and that compressive strain impacts this value. Taking these facts into account, we assume an initial neg- ative impact of static strain that is overcome with dynamic strain, having an optimal value of compressive strain rate above and below which the synthesis rate decays. The mathematical formulation for this dependence is depicted below:

$$\begin{aligned}k_{\text{GAG,s}} = k_{\text{GAG,s0}} (1 - \gamma_{\text{GAG}} \epsilon_{\text{min,prin}} + \delta_{\text{GAG}} \zeta_{\text{GAG}} \\ - \delta_{\text{GAG}} * | \epsilon_{\text{min,prin}} f - \zeta_{\text{GAG}} |)\end{aligned} \tag{20}$$

Despite the positive effect of moderate dynamic compressive strain in GAG synthesis, its retention in the ECM is not opti- mal due to the increased release to the culture media mediated by unconfined compression. However, with dynamic com- pression, in the calibration study, there is an increase in release that is not solely explained by fluid flow.

Therefore, we postulate that fluid flow affects directly the binding rate by mechanisms that may include removal of degraded GAGs:

$$k_{GAG,b} = k_{GAG,b0}(1 - \eta\epsilon_{min,prin} - \theta\sqrt{v_f}) \quad (21)$$

The concentration of GAGs is given in %w/w and is limited by the steady–state concentration, $GAG_{b,ss}$. The rate of synthesis of GAGs is given by $k_{GAG,s}$ *(*%w/w *(*cell $m^{-3})^{-1}$ $s^{-1}$*)*. The unbound fraction of GAG may diffuse to the culture medium as mediated by the diffusion coefficient, $D_{GAG}$ and by the fluid velocity, and is immobilized in the extracellular matrix at a temporal rate controlled by the binding coefficient, $k_{GAG,b}$ ($s^{-1}$) (Nikolaev et al. 2010; Haider et al. 2011).

We assume that the synthesized collagen is all bound to the extracellular matrix through linkage with the corresponding GAG fraction (Wilson et al. 2002; Catt et al. 2011). It is also assumed that collagen synthesis saturates at a given equilib- rium concentration:

$$\frac{\partial COL}{\partial t} = k_{COL}\rho_{cell}(COL_{ss} - COL) \quad (22)$$

Since the collagen fibers are fundamental to the tensile resistance of cartilage and are assumed to be aligned with the directions of the maximum principal strains, we assume that the synthesis is modulated by the maximum principal strain rate in order to accommodate the experimentally determined frequency-dependent effect on collagen and total protein synthesis rates (Lee and Bader 1997). We also hypothesize that there is an optimal value of maximum principal strain rate for collagen synthesis, below and above which the synthesis decreases. The model also incorporates the negative effect of the compressive strain, since previous works on static compression of tissue-engineered cartilage at different compression amplitudes have shown a decrease in collagen synthesis with an increase in compressive amplitude (Davis- son et al. 2002).

$$k_{COL} = k_{COL,0}(1 - \gamma_{COL}\epsilon_{min,prin} + \delta_{COL}\zeta_{COL} - \delta_{COL} * | \epsilon_{max,prin} f - \zeta_{COL} |) \quad (23)$$

### 2.1.7 Remodeling of mechanical properties

The influence of the concentration of bound GAG and COL on the remodeling of two important biphasic mechanical The influence of the concentration of bound GAG and COL on the remodeling of two important biphasic mechanical. For the Young modulus, a simple relationship adapted from Williamson et al. (2001) was employed, based on remodeling of the aggregate modu- lus ($H_a$) (Bandeiras et al. 2015).

$$H_a = R_{H_a,\mathrm{GAG}}\mathrm{GAG_b} + R_{H_a,\mathrm{COL}}\mathrm{COL} + H_{a,i} \tag{24}$$

The new aggregate modulus of the tissue is increased from the initial aggregate modulus of the construct without deposited ECM, $H_{a,i}$, linearly with bound GAG and collagen through the respective rates, $R_{H,\mathrm{GAG}}$ and $R_{H,\mathrm{GAG}}$(Pa (%w/w)$^{-1}$). Assuming that the Poisson coefficient, $\upsilon$, remains constant throughout the culture period, the new Young modulus is derived from the remodeled aggregate modulus by:

$$E_Y^- = H_a\frac{(1+\upsilon)(1-2\upsilon)}{1-\upsilon} \tag{25}$$

For the remodeling of permeability, the relationship in (3) is used with regard to the reduced fluid volume fraction obtained by the increase in the solid volume fraction due to biomass growth (cells and ECM) (Chung et al. 2007; Sacco et al. 2011). The conversion of concentrations and cell densities to solid volume fractions has followed the volume averaging approach presented in Haider et al. (2011).

## 2.2 Initial and boundary conditions

In order to replicate the construct dimensions used in the main dataset by Tsuang et al. (2008), 2D axisymmetric slices of 8 mm diameter 8 mm height cylinders were modeled in Abaqus 6.12 (Dassault Systèmes France) and meshed with 1326 pore pressure-stress

elements (Fig. 1). The number of elements was chosen after a mesh convergence analysis on the intrinsic mechanical parameters related to the model, which are the fluid velocity, void ratio, maximum and minimum principal strain. Convergence was reached when the output relative differences between the used mesh and an additional refinement are below 5 %. In a similar approach, the replication of the calibration dataset geometry by Lee and Bader (1997) was performed by modeling 2D axisymmetric slices of 5 mm diameter 5 mm height, meshed with 512 pore pressure-stress elements.

Regarding the boundary conditions, in unconfined compression and free swelling, the inferior surface (edge 1) is vertically restricted. Edge 2 is subjected to cyclic unconfined compression or in contact with the culture medium when in the free-swelling regime. The construct is symmetric about the center line (edge 3) in the axisymmetric configuration. Edge 4 is the lateral external face of the construct that allows for diffusion of nutrients from the culture medium in both settings. A zero pore pressure boundary condition is implemented in edge 4 to allow free fluid flow throughout the area in contact with fluid while the total solid stress is free to vary throughout the construct. Solutes and metabolites dissolved in the fluid (glucose, lactate and unbound GAG) are also free to flow in and out of the construct with the fluid. The plates that govern movement in edges 1 and 2 are assumed as impermeable and therefore do not allow fluid, cells or matrix flow in the *z* axis (Table 1).

It was considered that, in the beginning of culture, there was no extracellular matrix in the construct and that the initial mechanical properties were the ones of agarose 3 % w/w gels (Table 2). Additional initial conditions for the biosynthetic model are shown in Table 3.

### 2.3 Model parametrization

For this work, several parameters of the model were taken from the existing literature (Table 4). As a first approach, the appropriate parameters were estimated by fitting the

data of Lee and Bader (1997) to the ratios of cell proliferation and protein synthesis rates, as well as to the total GAG synthesis and the fraction of GAGs released to the culture medium (Figure S1, Tables S1–S2). The final unstrained concentrations of total GAG and collagen were fitted to data by Knight et al. (1998) in order to estimate the synthesis rates. Furthermore, the remodeling parameters for the Young modulus respective to GAG and collagen were estimated by fitting the Young modulus with GAG and collagen data presented in the work of Ng et al. (2005). Regarding the influence of mechanical parameters, whenever the data in Tsuang et al. (2008) allowed, new parameters were estimated for the 15 % compressive amplitude dataset in order to account for the different biological behavior of bovine and rat chondrocytes. These parameters were then used to carry the simulations for the 5 and 10 % compressive amplitudes for model validation.

### 2.4 Simulation procedure

The meshed constructs were subjected to 15 % static uncon- fined compression, as well as dynamic compression at 0.3, 1 and 3 Hz for the calibration dataset of Lee and Bader (1997) and to 5, 10 and 15 % dynamic unconfined compression at the frequencies of 0.5, 1, 2 and 3 Hz for the main case study of Tsuang et al. (2008). The simulations were run until steady state for each case in Abaqus in order to extract the values of the relevant intrinsic mechanical parameters at the compression maxima. Due to the applied boundary conditions for both the unstrained and strained conditions, considering two impermeable plates in $z$ 0 and $z$ height, and to the uniaxial cyclic unconfined compression, the results can be analyzed in one dimension only to extract the gradients and profiles of the intrinsic mechanical parameters and calculate the profiles of the biosynthetic model. These values were imported to MATLAB R2012b (Mathworks, USA) for model parametrization and simulation of the biosynthetic model. The models were run until the end of the culture periods (48 h for the calibration dataset and 24 h for the validation dataset). The numerical

ratios of the stimulated constructs relative to the unstrained controls for each case were calculated for cell densities, total GAG and collagen, as well as estimated for the Young modulus and permeability. In order to assess the influence of variations in the model parameters in the main outputs of the model, a sensitivity analysis was carried out to the unstrained condition for the baseline parameters and to the strained condition of 1 Hz, 10 % as a representative example of the impact of variations of parameters associated with mechanical stimulation.

## 3 Results

The radial distributions of fluid velocities, void ratios, maximum and minimum principal strains at the compression maxima are shown in Fig. 2 for each amplitude and frequency. With increasing amplitudes, the values of strains and fluid velocities in the periphery of the constructs increase, while the void ratio in the periphery of the constructs decreases. These distributions are driven by the free fluid flow boundary conditions for edge 4. For each compressive amplitude, the increase in amplitude causes a narrowing to more peripheral zones of the areas with lower maximum principal strains and void ratios than the core of the construct, while for fluid velocities, despite the increase in fluid velocity in the periphery mediated by the increasing frequency, the fluid velocity values decrease more abruptly from periphery to core.

The estimated concentrations of glucose and lactate in the culture medium throughout the simulation time show a significant depletion of glucose, with values of 2.35 mM, and significant release of lactate at a final concentration of 42 mM (Figure S2A). The radial distributions at 24 h show that there is some heterogeneity in the distribution of glucose, with a minimum concentration of 1.63 mM in the core of the construct. The lactate concentration is approximately uniform throughout all the construct, causing a significant

inhibition of cell proliferation in the constructs (Figure S2B). The different loading conditions have a higher relative impact in the availability of glucose than the production of lactate. For the majority of the loading conditions, there is a higher relative depletion of glucose compared to the same spatial points of the unstrained condition. The impact of dynamic loading in lactate distributions is not significant, and at all points, the concentrations are above the half-rate inhibitory concentration of 25 mM at the 24-h time point (Figure S3).

The average cell density in the control construct is esti- mated to grow until approximately 16 million cells/ml after 24 h. A decrease in growth is seen near the end of the culture period as a result of depletion of glucose and accumulation of lactate. For this short culture period, there is already a slight heterogeneity in the cell accumulation across the construct, with the cell density in the periphery approximately 5% higher than in the cores (Fig. 3a, b).

The model incorporating the shear stress rate dependency showed, for most of the frequency–amplitude combinations, a good agreement with the experimental data, with most of the numerical estimated averages being within the standard deviation of the experimental data. The frequency of increase in average cell densities with increasing stimulation frequency was reproduced for all amplitudes, and the decrease in cell densities with increasing stimulation amplitude for the frequency of 0.5 Hz was also reproduced. The average relative errors between the average experimental ratios of cell counts and the numerical predictions are of 3.1 % in the calibration dataset (15 %) and of 2.0 % for the validation datasets (5 and 10 %). The largest deviation from the experimental data was obtained for the 15%, 3-Hz condition, with the numerical average being approximately 8 % larger than the experimental average. This fact suggests that, for this experimental system, a peak in the shear stress rate for optimal synthesis might occur,

with a decrease in the proliferation stimulation for mechanical stimulation beyond this value (Fig. 4). The spatial ratios of the cell densities for all the load- ing conditions relatively to the unstrained control are shown in Fig. 5. For all the loading conditions, there is a slight decrease in the cell density relatively to the unloaded condition. In a limited area in the periphery of the constructs, close to 0.5 mm, the shear stress beneficial effect for cell proliferation overcomes the compressive strain limitation and, with the increase in frequency and amplitude, the accumulation of cells in the periphery increases up to 2.26 times the peripheral cell density in the unstrained condition. Therefore, the increase in average cell density in the higher frequency loaded conditions comes at the expense of an increase in spatial heterogeneity that may be deleterious in the long term for the establishment of tissues.

After 24 h of culture in the unstrained condition, the total average GAG concentration in the tissue is 1.55 $10^{-2}$ %w/w, with the synthesized values in the outer edge of the construct being approximately 3 % larger than in the core (Fig. 3c, d). The ratios of the total GAG concentrations in the construct show a good agreement with experimental data. The relative errors have a mean value of 1.1 % for the calibration data and of 4.3 % for the validation data. A maximum deviation of 6.7 % from experimental data was verified for the 5 %, 1-Hz condition. While the model generally allowed to predict the trends of evolution of GAG synthesis with frequency for a given amplitude, an overestimation of the total synthesis of GAGs for the 5 % condition was verified (Fig. 6). Regarding the spatial distributions of GAGs normalized to the unstrained construct values, the produced values are slightly below (up to 8 %) the ones produced for the unstrained condition in the cores of the construct, with a modest increase in GAG accumulation in the periphery of the constructs relatively to the cell density increase, with a maximum increase of 15 % in the periphery of the constructs.

This fact is related to the increased release of GAGs to the culture medium in regions of higher fluid flow (Fig. 7a, c, e). Under the model for the binding of released GAGs to the matrix calibrated with the data from Lee and Bader (1997), after 24 h, 19.46 % of the total synthesized GAGs were released to the culture medium. With cyclic compressive loading, for all the conditions, the released GAGs percentage is above this value and the percentage of release increases with the compressive amplitude, with maximum values of 36 % for the 15 % amplitude (Fig. 8). The impact of compressive frequency for each amplitude is not significant. Therefore, the increase in GAG synthesis rate seen for some loading conditions is counterbalanced by an increased release to culture medium.

After 24 h of culture in the unstrained condition, the aver- age collagen concentration in the tissue is $4.62\ 10^{-4}$ % w/w, with an heterogeneity from periphery to core after 24 h of 4 % (Fig. 3e, f). For all the loading conditions, the average ratios of collagen content are within the standard deviation of the mean of experimental data (Fig. 9). The average relative errors were of 2.1 % in the calibration data and 3.6 % in the validation data. The numerical deviations from the experimental mean go up to 6.6 % for the 5 %, 0.5-Hz condition. The model reproduced the trend of decreasing collagen synthesis with increasing frequency for the 15 % amplitude, while for the other amplitudes such a marked trend is not obtained in the data. As seen for the GAG production, the model also overestimates the collagen production at 5 % amplitudes. The spatial distributions (Fig. 7b, d, f) indicate that, in agreement with lower cell densities, the collagen content in the cores is up to 11 % lower than in the unstrained condition, with spatial heterogeneity growing with amplitude and frequency. In the periphery of the constructs, an increased accumulation of collagen (up to 57 %) is verified for all the strained conditions.

After 24 h, the synthesized ECM concentrations are fairly negligible for the remodeling

of mechanical properties, with an increase of only 0.3 % in the average compressive Young modulus and a decrease of 3.8 % in the average permeability, with negligible spatial heterogeneities. However, very slight differences in the average mechanical parameters can be discerned, with the highest Young modulus estimated for the condition of 5 %, 3 Hz as a combination of higher GAG synthesis with moderate release to the culture medium and the lowest permeability estimated for 15 %, 3 Hz as a result of the highest estimated cell proliferation (Figure S4).

Finally, in order to evaluate the sensitivity of the model to variations in the key parameters that influence the key outputs of the model (cell density, GAG, % GAG released and collagen), a sensitivity analysis was carried out to the baseline parameters without the effect of mechanical stimulation in the unstrained condition (Table S3), accounting for an impact of 50 % variation on the model parameters. The parameter that caused higher variation in the respective out- put is the GAG binding rate, for which a decrease of 50 % leads to an increase of 82 % of the relative released GAGs to the culture medium. Furthermore, in order to study the impact of the parameters that influence the response of the culture to mechanical stimulation, a sensitivity analysis of these parameters for the 1 Hz, 10 % culture was performed as a representative example (Table S4). For this particular condition, the most important parameters to control are the parameters related to the GAG binding rate modulation, especially parameter $\theta$ that controls the evolution of the binding rate with the fluid velocity.

## 4 Discussion

The main goal of this study was to apply a fully coupled mathematical model to analyze the impact of several cyclic unconfined compression regimes on the spatial and temporal dynamics of variables that were not measured experimentally in Tsuang et al. (2008),

such as glucose and lactate, fraction of GAGs released to the culture medium and tissue permeability, and to assess the validity of the model for several combinations of amplitude and frequency by comparison with the average experimental outputs of cell density, total GAGs and collagen. This work provides the first validated extension for mechanically loaded cultures of the validated model for free-swelling cultures presented in Bandeiras et al. (2015) and takes on similar assumptions from the theoretical simulation efforts for compression, shear, bending and hydrostatic pressure regimes (Bandeiras et al. 2014a, b).

The proposed mechanistic models allowed to reproduce the experimental frequency-dependent trends in the rates of synthesis of the measured entities, with average relative errors of the fitting of 3.2 % and maximum relative errors of 8.3 %. The validation of the model with the 5 and 10 % amplitude datasets of (Tsuang et al. 2008) at several different frequencies was also successful, with average relative errors values of up to 4.3 % and maximum relative error of 6.7 %. These error values are reasonable when considering the complexity of the model and of the underlying biological phenomena, and most of the numerical means are located within a standard deviation of the experimental mean. These results are a good starting point to use this approach for the simulation of different intermittent and continuous unconfined compression regimes for longer culture periods and also to study the application to other complex regimes.

The numerical approach also allows to provide quan-itative spatial information on the intrinsic mechanical parameters and quantities that were not measured by the experimental studies. The model determines, as expected due to the higher nutrient availability and the higher fluid flow and shear stress, more growth and synthesis activity in the periphery of the constructs. These results are consistent with experimental studies that compared the availability of GAGs and collagens in the periphery and cores

of the constructs (Buschmann et al. 1999; Mesallati et al. 2013). The estimated distributions of glucose and lactate in the constructs are consistent with the initial seeding density and other published works (Sengers et al. 2005). After only 24 h in culture, very high lactate concentrations are achieved throughout the whole construct with considerable glucose depletion. For this reason, a limitation in growth starts to be noticeable. The established model can be used to simulate different culture media exchange protocols to avoid cell proliferation saturation with accumulation of toxic by-products. A considerable limitation of continuous compressive loading is the increased release of GAGs to the culture medium, which is a deleterious factor for the establishment of good mechanical properties. After 24 h in unconfined compression reaches values of up to 36 % of the total GAGs produced, while for the unstrained condition 19.5 % of total GAGs are unbound. These considerable differences are highlighted by the very short culture time and the slow process of binding to the matrix, but are enough to induce some differences in the estimated mechanical properties. The highest estimated compressive Young modulus is simulated for the 5 %, 3-Hz condition. This comes as a combination of a moderate release of GAGs (23.6 %) and improvement in the GAG synthesis relatively to the unstrained condition. Therefore, the applica tion of the model under longer-term intermittent stimuli and validation with measurements of the Young modulus will be valuable to predict the role of GAG release on different conditions and establish a good combination between synthesis and retention. The differences in remodeling of permeability between conditions are also not significant after 24 h but favor conditions with higher cell proliferation. With a very small amount of ECM at this time point, promoting loading conditions that favor a very fast cell proliferation may be favorable, but this regime needs to be balanced with regimes that pro- mote high matrix synthesis per cell combined with limiting nutrient availability

and release of matrix components.

Regarding the model for chondrocyte metabolism, we have only estimated the dynamics of glucose and lactate transport and uptake. Another important metabolite used in previous modeling studies is oxygen, which was also accounted for in cell proliferation models (Nava et al. 2013; Sengers et al. 2004b; Sacco et al. 2011). The model account- ing for a fully anaerobic metabolism of glucose and the impact of glucose and lactate in cell proliferation, combined with the shear stress dependency, provided a good approxi- mation to the cell density ratios for the several mechanical stimulation conditions. Additionally, by comparing our glu- cose metabolism data with previous studies, there is no evidence of an influence of oxygen concentration on glu- cose metabolism for the glucose concentration and seeding density simulated after 24 h through complex effects like the Crabtree or negative Pasteur effects (Zhou et al. 2008; Sen- gers et al. 2004b; Lee and Urban 1997). Under these facts, we assumed that, throughout the experiment, the glucose metabolism is anaerobic and that oxygen does not impact significantly the cell density profiles. However, for longer culture times and higher seeding densities, a model includ- ing oxygen may need to be applied.

In this model we also have not included the effect of solutes in matrix synthesis or in the maintenance of chondrocyte phenotype, unlike other previously reported works that used culture times of several weeks to validate the models (Niko- laev et al. 2010; Myers and Ateshian 2014; Li et al. 2014). While previous studies report that hypoxia favors the main- tenance and differentiation into a chondrocytic phenotype, (Buckley et al. 2010; Foldager et al. 2011) the evidence that 3D cultures in hydrogels maintain and promote redifferen- tiation of dedifferentiated chondrocytes (Benya and Shaffer 1982; Takahashi et al. 2007) combined with the short culture time simulated in this study leads us to assume that there are no significant oxygen-mediated modifications in the cell phe-

notype. Regarding the effect of solutes in matrix synthesis, previous modeling efforts reported a linear increase of GAG synthesis with oxygen concentration (Nikolaev et al. 2010; Obradovic et al. 2000), while other article postulated a thresh- old of 8 % oxygen tension above which collagen synthesis is favored and below which proteoglycan synthesis increases, as long as there is enough oxygen to avoid necrotic core formation (Li et al. 2014). The absence of histological experi- mental measures to validate these predictions in combination with the mechanical factors considered herein would hinder the correct determination of the coupled effects of oxygen and mechanical factors in matrix synthesis, suggesting that validation of a combined mechanical and oxygen-mediated matrix synthesis needs to be carried out with a long-term culture experiment.

In the cell proliferation model, an overestimation of cell density for the 15 %, 3-Hz condition was verified, while the more favorable experimental conditions of 10 %, 2–3 Hz were underestimated. This result suggests that, under cyclic unconfined compression, there is an optimal value, or range of values, for proliferation, with values above which inhibiting the proliferation. A previous modeling effort for growth under perfusion reported a piecewise shear stress modulation of cell proliferation, with maximum proliferation rates in the 0.1–0.6 Pa range and complete growth inhibition above 1 Pa (Nava et al. 2013). The maximum values identified for shear stress were within the favorable range. This piecewise model has the limitation that no experimental data for validation were available between 0.1 and 0.6 Pa. Therefore, further val- idation of models accounting for an optimal range of shear stress values, with experimental values available within a wider range of stresses, is necessary for a more exact model development.

While most of the model outputs are fairly robust with respect to changes in the model parameters, changes of up to 82 % in the unbound GAG fraction are identified when chang-

ing the parameters of the GAG binding model by 50%. Apart from this, upon model calibration, the trend of slight decrease in the released GAG fraction with increasing stimu- lation frequency was not reproduced, since the released GAG percentage is higher at 1 Hz than at 0.3 Hz and the decrease in release rate is more pronounced at 3 Hz. While we con- sider that this difference is not significant since data show a considerable experimental error and the simulation time is very short (48 h with continuous dynamic loading), we also consider that the formulation of the relationship between binding and intrinsic mechanical parameter needs to be fur- ther developed. This is of particular importance given the fact that the relationship for GAG binding was developed for the agarose 3 % scaffold and may need to be recalibrated or reformulated for different scaffold materials due to different physicochemical and mechanical properties. Further model validation concerning the rate of binding of GAGs to the ECM, with more combinations of amplitude and frequency, together with longer-term intermittent and continuous load- ing conditions will be valuable for this goal.

As a final remark, in this work, the constitutive rela- tionship used assumes a linear elastic solid with isotropic properties. With longer culture times, collagen fibers grow oriented according to directions dictated by the orienta- tion and magnitude of maximum principal strains (Wilson et al. 2007). Therefore, the model needs to accommodate the anisotropy in the mechanical properties arising from this structure in order to better resemble the stress–strain behavior of growing cartilage (Pierce et al. 2013).

In short, a fully coupled mathematical formulation account- ing for simultaneous simulation of solute transport and uptake, cell proliferation, extracellular matrix production and remodeling mechanical properties accounting for the effect of mechanical stimulation on the rates of synthesis and proliferation was developed and validated for several ampli- tudes and frequencies of unconfined cyclic compression. The model

showed a good agreement with the experimental data and allowed to capture the main phenomena associated with spatial and temporal growth of tissue-engineered carti- lage under short-term loading and estimate the distributions of variables not experimentally measured. This formulation can be used as well to predict the effect of other culture conditions and to optimize experimental designs. Further model development and validation involve the application of the model for other hydrogel and chondrocyte experi- mental systems, longer-term loading conditions, other types of mechanical stimulation, the refinement of mechanical loading dependencies and the inclusion of an anisotropic con- stitutive relationship to account for the orientation of collagen fibers in a long-term tissue-engineered cartilage culture.

**Acknowledgments:**

This work is supported by FCT Fundação para a Ciência e Tecnologia with the reference Project PTDC/EMS-TEC/3263/2014 and by FEDER through the Programa Operacional Competitividade e Internacionalização - Project POCI-01-0145-FEDER-016574.

**Compliance with ethical standards**

**Conflict of interest.** The authors declare that they have no conflict of interest

**References**

Bandeiras C, Completo A (2013) Comparison between constitutive models for the solid phase of biphasic agarose/chondrocytes con- structs for knee cartilage engineering. Comput Methods Biomech Biomed Eng 16(sup1):262–263

Bandeiras C, Completo A (2015) Comparison of mechanical parameters between tissue-engineered and native cartilage: a numerical study. Comput Methods Biomech Biomed Eng 18(sup1):1876–1877

Bandeiras C, Completo A, Ramos A (2014a) Compression, shear and bending on tissue-engineered cartilage: a numerical study. Comput Methods Biomech Biomed Eng 17(sup1):2–3

Bandeiras C, Completo A, Ramos A (2014b) Simulation of remodeling of tissue engineered condylar cartilage under static hydrostatic pressure. Biodental Eng III:83

Bandeiras C, Completo A, Ramos A (2015) Influence of the scaffold geometry on the spatial and temporal evolution of the mechanical properties of tissue-engineered cartilage: insights from a mathe- matical model. Biomech Model Mechanobiol 14(5):1057–1070

Benya PD, Shaffer JD (1982) Dedifferentiated chondrocytes reexpress the differentiated collagen phenotype when cultured in agarose gels. Cell 30(1):215–224

Buckley CT, Vinardell T, Kelly DJ (2010) Oxygen tension differen- tially regulates the functional properties of cartilaginous tissues engineered from infrapatellar fat pad derived mscs and articular chondrocytes. Osteoarthr Cartil 18(10):1345–1354

Buschmann MD, Kim YJ, Wong M, Frank E, Hunziker EB, Grodzinsky AJ (1999) Stimulation of aggrecan synthesis in cartilage explants by cyclic loading is localized to regions of high interstitial fluid flow. Arch biochem Biophys 366(1):1–7

Catt C, Schuurman W, Sengers B, Van Weeren P, Dhert W, Please C, Malda J (2011) Mathematical modelling of tissue formation in chondrocyte filter cultures. Eur Cell Mater 22:377–392

Chung C, Yang C, Chen C (2006) Analysis of cell growth and diffusion in a scaffold for cartilage tissue engineering. Biotechnol Bioeng 94(6):1138–1146

Chung C, Chen C, Chen C, Tseng C (2007) Enhancement of cell growth in tissue-engineering constructs under direct perfusion: modeling and simulation. Biotechnol Bioeng 97(6):1603–1616.

Costa KD, Ho MM, Hung CT, (2003) Multi-scale measurement of mechanical properties of soft samples with atomic force microscopy. In: 2003 summer bioengineering conference. Florida, Key Biscaine, p 2

Davisson T, Kunig S, Chen A, Sah R, Ratcliffe A (2002) Static and dynamic compression modulate matrix metabolism in tissue engi- neered cartilage. J Orthop Res 20(4):842–848

Dijkman P, Bader D, Lee D, Chowdhury T, Heywood H (2005) Glucose utilisation of chondrocytes, with or without loading. In: External placement report, Technical University of Eindhoven and Queen Mary University, London

Evans RC, Quinn TM (2006) Dynamic compression augments intersti- tial transport of a glucose-like solute in articular cartilage. Biophys J 91(4):1541–1547

Foldager CB, Nielsen AB, Munir S, Ulrich-Vinther M, Søballe K, Bünger C, Lind M (2011) Combined 3D and hypoxic culture improves cartilage-specific gene expression in human chondro- cytes. Acta Orthop 82(2):234–240

Galban CJ, Locke BR (1999) Analysis of cell growth kinetics and substrate diffusion in a polymer scaffold. Biotechnol Bioeng 65(2):121–132

Gao X, Zhu Q, Gu W (2015) Analyzing the effects of mechanical and osmotic loading on glycosaminoglycan synthesis rate in cartilagi- nous tissues. J Biomech 48(4):573–577

Gardiner B, Smith D, Pivonka P, Grodzinsky A, Frank E, Zhang L (2007) Solute transport in cartilage undergoing cyclic deformation. Comput Methods Biomech Biomed Eng 10(4):265–278

Haider MA, Olander JE, Arnold RF, Marous DR, McLamb AJ, Thomp- son KC, Woodruff WR, Haugh JM (2011) A phenomenological mixture model for biosynthesis and linking of cartilage extracellu- lar matrix in scaffolds seeded with chondrocytes. Biomech Model Mechanobiol 10(6):915–924

Hossain MS, Bergstrom D, Chen X (2015) Modelling and simulation of the chondrocyte cell growth, glucose consumption and lactate production within a porous tissue scaffold inside a perfusion biore- actor. Biotechnol Rep 5:55–62

Hung CT, Mauck RL, Wang CCB, Lima EG, Ateshian GA (2004) A paradigm for functional tissue engineering of articular cartilage via applied physiologic deformational loading. Ann Biomed Eng 32(1):35–49

Khoshgoftar M, Wilson W, Ito K, van Donkelaar CC (2013) The effect of tissue-engineered cartilage biomechanical and biochemical prop- erties on its post-implantation mechanical behavior. Biomech Model Mechanobiol 12(1):43–54

Kisiday JD, Jin M, DiMicco MA, Kurz B, Grodzinsky AJ (2004) Effects of dynamic compressive loading on chondrocyte biosynthesis in self-assembling peptide scaffolds. J Biomech 37(5):595–604

Knight M, Lee D, Bader D (1998) The influence of elaborated pericel- lular matrix on the deformation of isolated articular chondrocytes cultured in agarose. Biochimica et Biophysica Acta (BBA)- Molecular. Cell Res 1405(1):67–77

Lee DA, Bader DL (1997) Compressive strains at physiological frequen- cies influence the metabolism of chondrocytes seeded in agarose. J Orthop Res 15(2):181–188

Lee RB, Urban JP (1997) Evidence for a negative pasteur effect in articular cartilage. Biochem J 321(1):95–102

Lelli C, Sacco R, Causin P, Raimondi MT (2015) A poroelastic mixture model of mechanobiological processes in tissue engineering. part I: mathematical formulation. arXiv p 1512.02182

Li S, Oreffo RO, Sengers BG, Tare RS (2014) The effect of oxygen tension on human articular chondrocyte matrix synthesis: integra- tion of experimental and computational approaches. Biotechnol Bioeng 111(9):1876–1885

Lin WY, Chang YH, Wang HY, Yang TC, Chiu TK, Huang SB, Wu MH (2014) The study of the frequency effect of dynamic com

pressive loading on primary articular chondrocyte functions using a microcell culture system. BioMed Res Int 2014:762570

Mauck RL, Hung CT, Ateshian GA (2003) Modeling of neutral solute transport in a dynamically loaded porous permeable gel: implica- tions for articular cartilage biosynthesis and tissue engineering. J Biomech Eng 125(5):602–614

Mesallati T, Buckley CT, Nagel T, Kelly DJ (2013) Scaffold architecture determines chondrocyte response to externally applied dynamic compression. Biomech Model Mechanobiol 12(5):889–899

Mow VC, Kuei S, Lai WM, Armstrong CG (1980) Biphasic creep and stress relaxation of articular cartilage in compression: theory and experiments. J Biomech Eng 102(1):73–84

Myers K, Ateshian GA (2014) Interstitial growth and remodeling of biological tissues: tissue composition as state variables. J Mech Behav Biomed Mater 29:544–556

Nava MM, Raimondi MT, Pietrabissa R (2013) A multiphysics 3D model of tissue growth under interstitial perfusion in a tissue-engineering bioreactor. Biomech Model Mechanobiol 12(6):1169–1179

Ng KW, Wang CCB, Mauck RL, Kelly TAN, Chahine NO, Costa KD, Ateshian GA, Hung CT (2005) A layered agarose approach to fabricate depth-dependent inhomogeneity in chondrocyte-seeded constructs. J Orthop Res 23(1):134–141

Nikolaev N, Obradovic B, Versteeg HK, Lemon G, Williams DJ (2010) A validated model of gag deposition, cell distribution, and growth of tissue engineered cartilage cultured in a rotating bioreactor. Biotechnol Bioeng 105(4):842–853

Obradovic B, Meldon JH, Freed LE, Vunjak-Novakovic G (2000) Gly- cosaminoglycan deposition in engineered cartilage: experiments and mathematical model. AIChE J 46(9):1860–1871

Pierce DM, Ricken T, Holzapfel GA (2013) A hyperelastic biphasic fibre-reinforced model of articular cartilage considering distrib- uted collagen fibre orientations: continuum basis, computational aspects and applications. Comput Methods Biomech Biomed Eng 16(12):1344–1361

Sacco R, Causin P, Zunino P, Raimondi MT (2011) A multi- physics/multiscale 2D numerical simulation of scaffold-based cartilage regeneration under interstitial perfusion in a bioreactor. Biomech Model Mechanobiol 10(4):577–589

Sengers B, Van Donkelaar C, Oomens C, Baaijens F (2004a) The local matrix distribution and the functional development of tis- sue engineered cartilage, a finite element study. Ann Biomed Eng 32(12):1718–1727

Sengers BG, Oomens CW, Baaijens FP (2004b) An integrated finite- element approach to mechanics, transport and biosynthesis in tissue engineering. J Biomech Eng 126(1):82–91

Sengers BG, Heywood HK, Lee DA, Oomens CW, Bader DL (2005) Nutrient utilization by bovine articular chondrocytes: a com- bined experimental and theoretical approach. J Biomech Eng 127(5):758–766

Takahashi T, Ogasawara T, Asawa Y, Mori Y, Uchinuma E, Takato T, Hoshi K (2007) Three-dimensional microenvironments retain chondrocyte phenotypes during proliferation culture. Tissue Eng 13(7):1583–1592

Tasci A, Ferguson SJ, Büchler P (2011) Numerical assessment on the effective mechanical stimuli for matrix-associated metabolism in chondrocyte-seeded constructs. J Tissue Eng Regen Med 5(3):210–219

Tsuang YH, Lin Y, Chen L, Cheng C, Sun JS (2008) Effect of dynamic compression on in vitro chondrocyte metabolism. Int J Artif Organs 31(5):439–449

Williamson AK, Chen AC, Sah RL (2001) Compressive properties and function composition relationships of developing bovine articular cartilage. J Orthop Res 19(6):1113–1121

Wilson CG, Bonassar LJ, Kohles SS (2002) Modeling the dynamic composition of engineered cartilage. Arch Biochem Biophys 408(2):246–254

Wilson W, Huyghe J, Van Donkelaar C (2007) Depth-dependent com- pressive equilibrium properties of articular cartilage explained by its composition. Biomech Model Mechanobiol 6(1–2):43–53

Wimmer M, Guenther H, Grad S, Lee C, Haenni M, Gogolewski S, Alini M (2003) Numerical simulation as a tool to evaluate load- ing regimes for tissue engineering. In:

49th annual meeting of the orthopaedic research society, New Orleans, LA

Zhang L, Szeri A (2005) Transport of neutral solute in articular cartilage: effects of loading and particle size. Proc R Soc Lond A Math Phys Eng Sci R Soc 461:2021–2042

Zhou S, Cui Z, Urban JP (2008) Nutrient gradients in engineered carti- lage: metabolic kinetics measurement and mass transfer modeling. Biotechnol Bioeng 101(2):408–421

**List of Tables**

**Table 1** Boundary conditions

| Edge | Glucose | Cell density | GAG,ub | Collagen |
|---|---|---|---|---|
| 1 | $\frac{\partial c_{\mathrm{glc}}}{\partial z} = 0$ | $\frac{\partial \rho_{\mathrm{cell}}}{\partial z} = 0$ | $\frac{\partial \mathrm{GAG_{ub}}}{\partial z} = 0$ | $\frac{\partial \mathrm{COL}}{\partial z} = 0$ |
| 2 | $\frac{\partial c_{\mathrm{glc}}}{\partial z} = 0$ | $\frac{\partial \rho_{\mathrm{cell}}}{\partial z} = 0$ | $\frac{\partial \mathrm{GAG_{ub}}}{\partial z} = 0$ | $\frac{\partial \mathrm{COL}}{\partial z} = 0$ |
| 3 | Free diffusion | Free diffusion | Free diffusion | Free diffusion |
| 4 | Free diffusion | $\frac{\partial \rho_{\mathrm{cell}}}{\partial x} = 0$ | Free diffusion | $\frac{\partial \mathrm{COL}}{\partial x} = 0$ |

**Table 2** Initial mechanical properties

| Parameter | Value | References |
|---|---|---|
| $E_{\mathrm{Y}}^{-}$ | 24.3 kPa | Costa et al. (2003) |
| $\upsilon$ | 0.30 | Tasci et al. (2011) |
| $k$ | $5 \times 10^{-12}\,\mathrm{m^4\,N^{-1}s^{-1}}$ | Tasci et al. (2011) |
| $e_{\mathrm{o}}$ | 4.0 | Tasci et al. (2011) |

**Table 3** Initial conditions for the biosynthetitc model to replicate (Tsuang et al. 2008)

| Variable | Value |
|---|---|
| Glucose, medium | 25 mM |
| Glucose, construct | 12.5 mM |
| Lactate | 0 mM |
| Cell density | $10 \times 10^{12}\,\mathrm{cells\,m^{-3}}$ |
| GAG | 0 % w/w |
| Collagen | 0 % w/w |

**Table 4** Parameters for the biosynthetic model

| Parameter | Value | References |
|---|---|---|
| $D_{glc,water}$ | $9.66 \times 10^{-12}\ m^2\ s^{-1}$ | Mauck et al. (2003) |
| $V_{max,glc}$ | $1.87 \times 10^{-17}$ mol cell $^{-1}\ s^{-1}$ | Sengers et al. (2005) |
| $K_{m,glc}$ | $5 \times 0.35$ mM | Sengers et al. (2005) |
| $D_{cell,tissue}$ | $1.7 \times 10^{-14}\ m^2\ s^{-1}$ | Chung et al. (2006) |
| $\mu_{max}$ | $1.87 \times 10^{-5}\ s^{-1}$ | Derived from Dijkman et al. (2005) |
| $R_{death}$ | $3.3 \times 10^{-7}\ s^{-1}$ | Chung et al. (2007) |
| $\alpha$ | 2.22 | Estimated from Tsuang et al. (2008) |
| $\beta$ | 6.46 s $Pa^{-1}$ | Estimated from Tsuang et al. (2008) |
| $K_{glc}$ | 12.8 mM | Hossain et al. (2015) |
| $K_{lac}$ | 25.6 mM | Hossain et al. (2015) |
| $D_{GAG,water}$ | $7.0 \times 10^{-11}\ m^2\ s^{-1}$ | Obradovic et al. (2000) |
| $GAG_{b,ss}$ | 10 % w/w | Bandeiras et al. (2015) |
| $COL_{ss}$ | 2.25 % w/w | Bandeiras et al. (2015) |
| $k_{GAG,s}$ | $1.31 \times 10^{-21}$ % w/w (cell $m^{-3})^{-1}\ s^{-1}$ | Estimated from Knight et al. (1998) |
| $k_{GAG,b}$ | $6.07 \times 10^{-5}\ s^{-1}$ | Estimated from Lee and Bader (1997) |
| $k_{COL}$ | $1.74 \times 10^{-22}$ % w/w (cell $m^{-3})^{-1}\ s^{-1}$ | Estimated from Knight et al. (1998) |
| $\gamma_{GAG}$ | $2.08 \times 10^{-2}$ | Estimated from Tsuang et al. (2008) |
| $\delta_{GAG}$ | 1.22 | Estimated from Tsuang et al. (2008) |
| $\zeta_{GAG}$ | 0.11 | Estimated from Tsuang et al. (2008) |
| $\eta$ | 1.94 | Estimated from Lee and Bader (1997) |
| $\theta$ | 377.56 | Estimated from Lee and Bader (1997) |
| $\gamma_{COL}$ | −0.36 | Estimated from Tsuang et al. (2008) |
| $\delta_{COL}$ | 1.08 | Estimated from Tsuang et al. (2008) |
| $\zeta_{COL}$ | $2.23 \times 10^{-2}$ | Estimated from Tsuang et al. (2008) |
| $R_{H_a,GAG}$ | 8.6 kPa % w/w | Estimated from Ng et al. (2005) |
| $R_{H_a,COL}$ | 0.2 kPa % w/w | Estimated from Ng et al. (2005) |

**List of figures:**

**Figures**

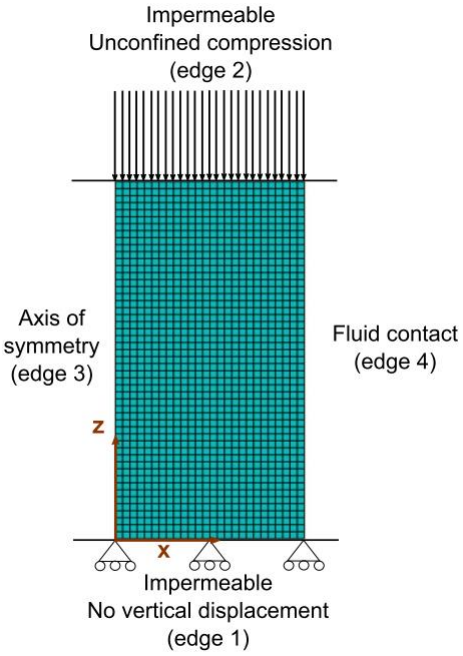


**Fig. 1**

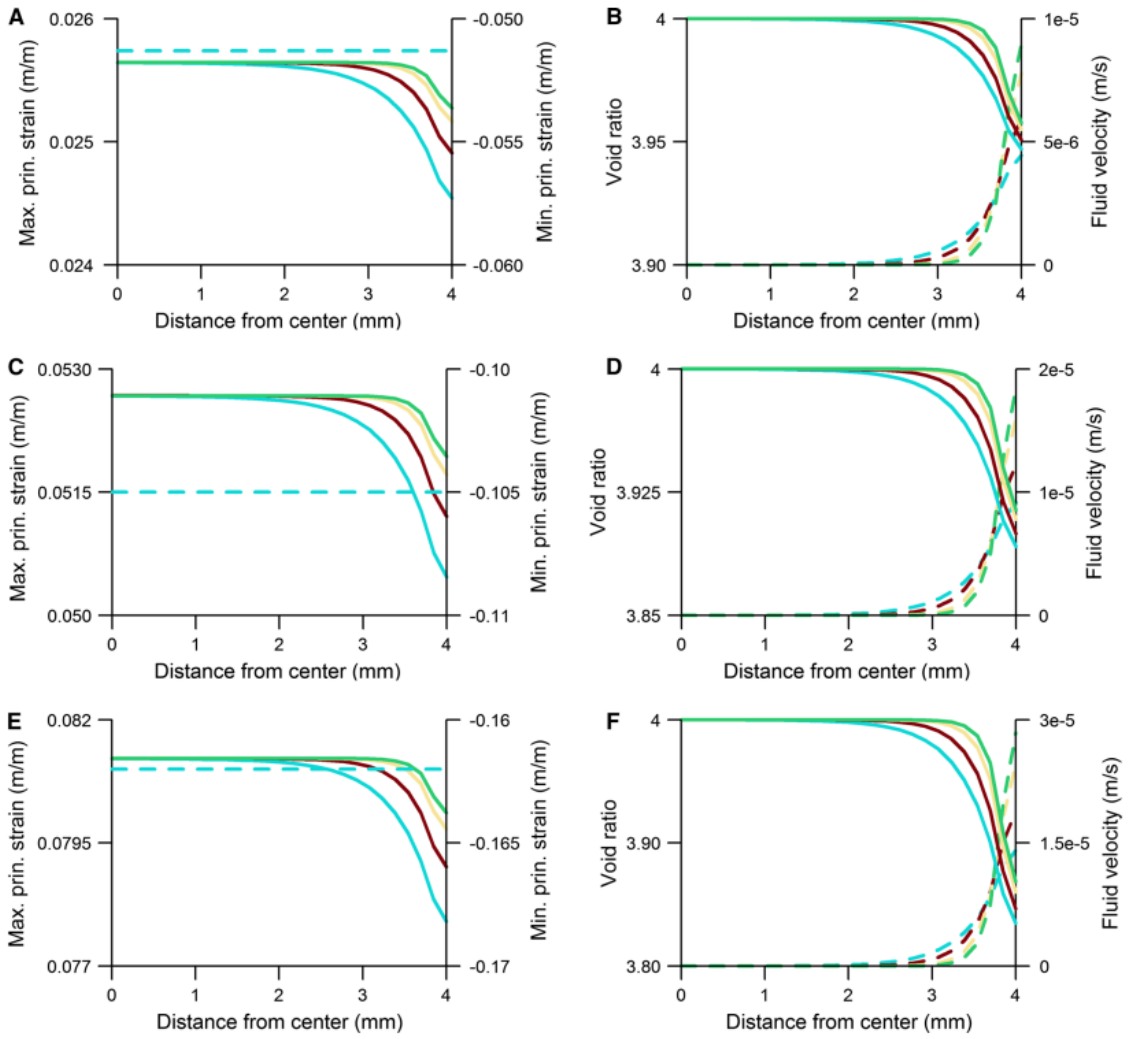
A
Max. prin. strain (m/m)
0.026
0.025
0.024
-0.050
-0.055
-0.060
Min. prin. strain (m/m)
Distance from center (mm)
B
Void ratio
4
3.95
3.90
1e-5
5e-6
0
Fluid velocity (m/s)
Distance from center (mm)
C
Max. prin. strain (m/m)
0.0530
0.0515
0.050
-0.10
-0.105
-0.11
Min. prin. strain (m/m)
Distance from center (mm)
D
Void ratio
4
3.925
3.85
2e-5
1e-5
0
Fluid velocity (m/s)
Distance from center (mm)
E
Max. prin. strain (m/m)
0.082
0.0795
0.077
-0.16
-0.165
-0.17
Min. prin. strain (m/m)
Distance from center (mm)
F
Void ratio
4
3.90
3.80
3e-5
1.5e-5
0
Fluid velocity (m/s)
Distance from center (mm)

**Fig. 2**

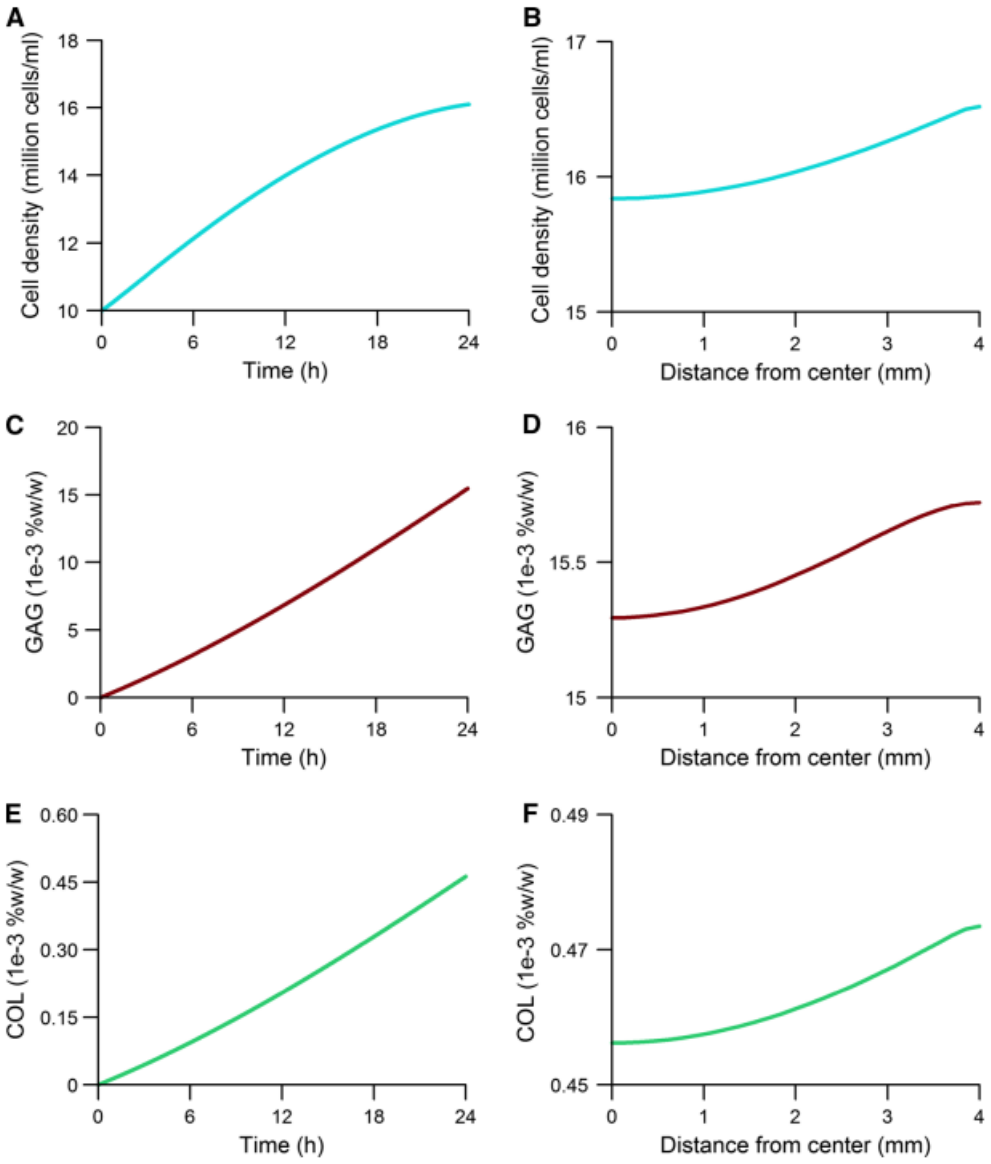
A
Cell density (million cells/ml)
18
16
14
12
10
0
6
12
18
24
Time (h)
B
Cell density (million cells/ml)
17
16
15
0
1
2
3
4
Distance from center (mm)
C
GAG (1e-3 %w/w)
20
15
10
5
0
0
6
12
18
24
Time (h)
D
GAG (1e-3 %w/w)
16
15.5
15
0
1
2
3
4
Distance from center (mm)
E
COL (1e-3 %w/w)
0.60
0.45
0.30
0.15
0
0
6
12
18
24
Time (h)
F
COL (1e-3 %w/w)
0.49
0.47
0.45
0
1
2
3
4
Distance from center (mm)

**Fig. 3**

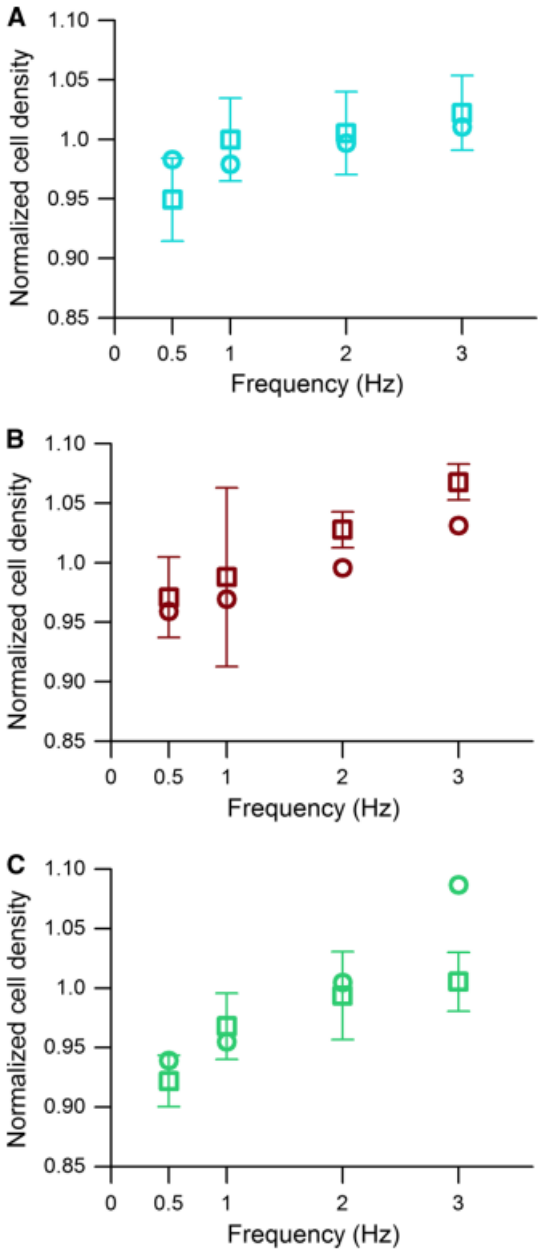
A
B
C
Normalized cell density
1.10
1.05
1.0
0.95
0.90
0.85
0
0.5
1
2
3
Frequency (Hz)

**Fig. 4**

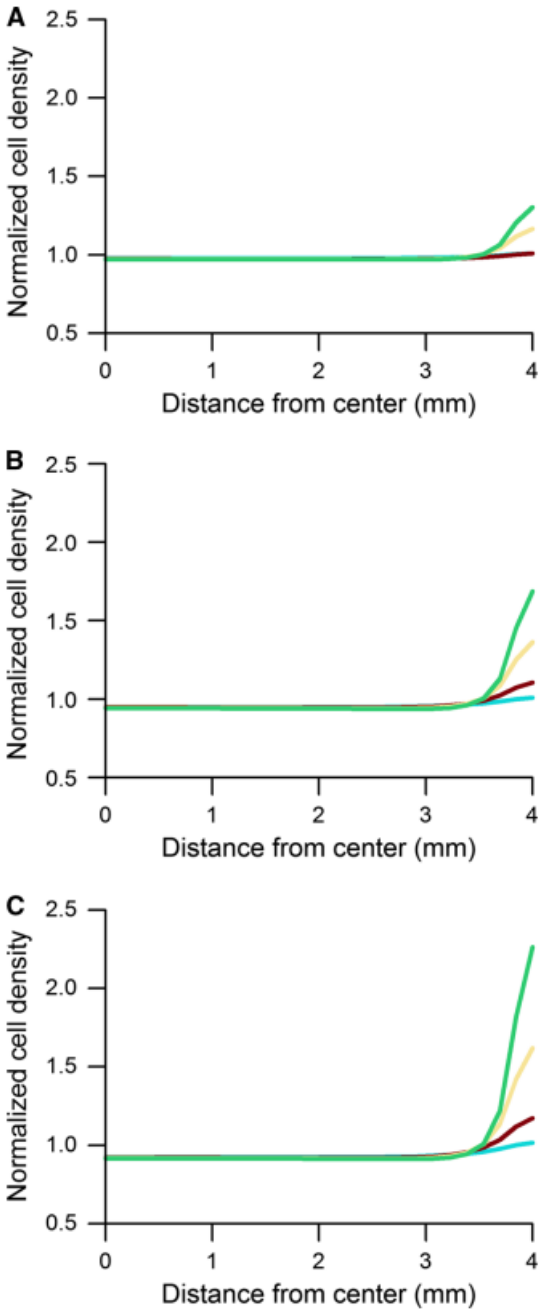
A
Normalized cell density
2.5
2.0
1.5
1.0
0.5
0
1
2
3
4
Distance from center (mm)
B
Normalized cell density
2.5
2.0
1.5
1.0
0.5
0
1
2
3
4
Distance from center (mm)
C
Normalized cell density
2.5
2.0
1.5
1.0
0.5
0
1
2
3
4
Distance from center (mm)

**Fig. 5**

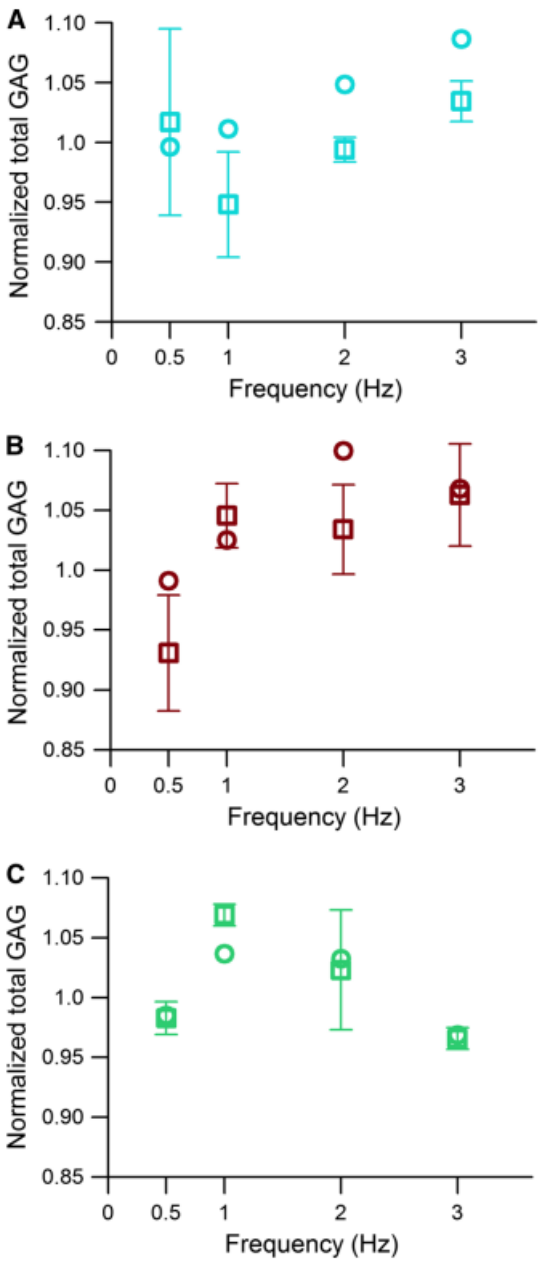
A
B
C
Normalized total GAG
1.10
1.05
1.0
0.95
0.90
0.85
0
0.5
1
2
3
Frequency (Hz)

**Fig. 6**

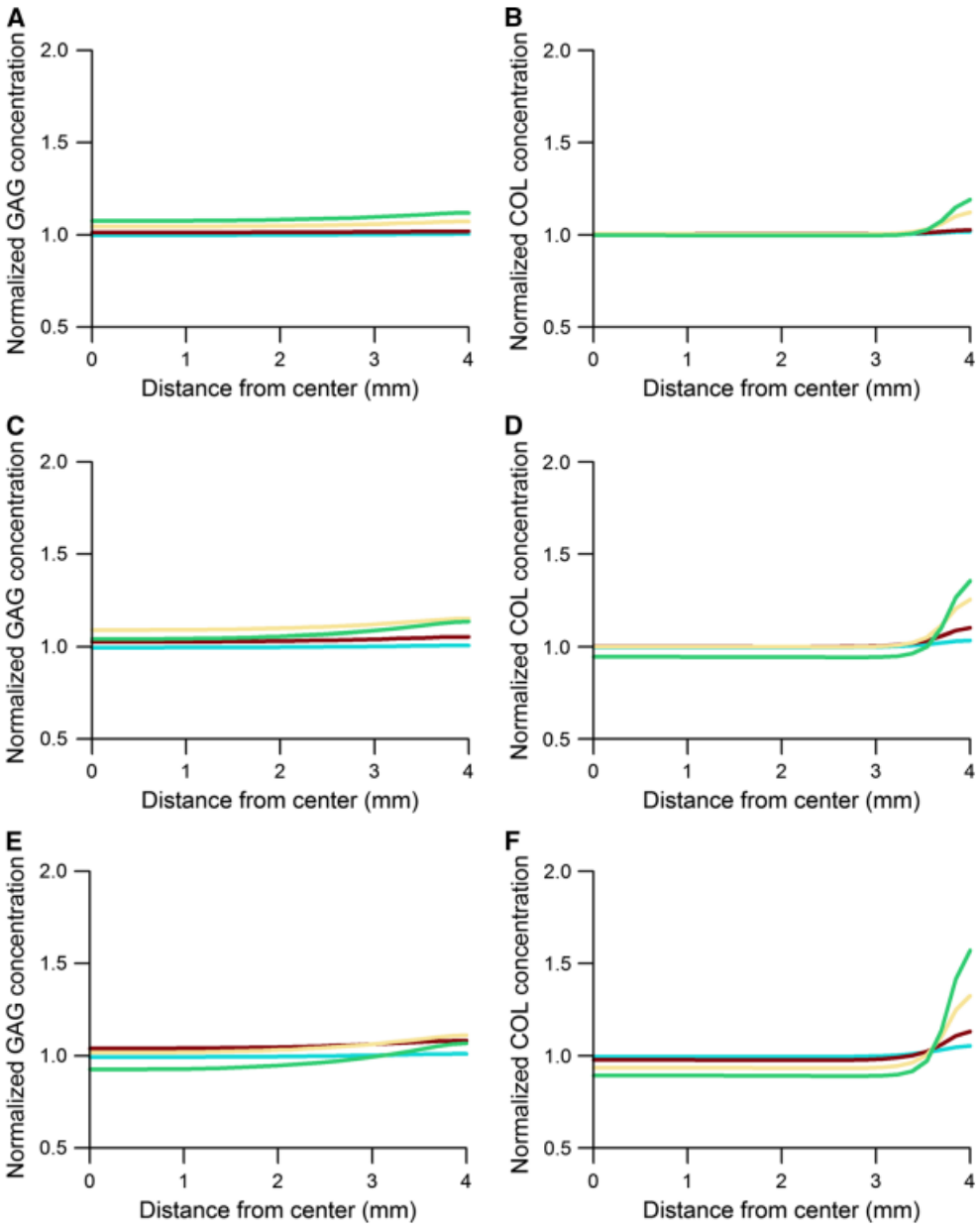
A
B
C
D
E
F
Normalized GAG concentration
Normalized COL concentration
2.0
1.5
1.0
0.5
0
1
2
3
4
Distance from center (mm)

**Fig. 7**

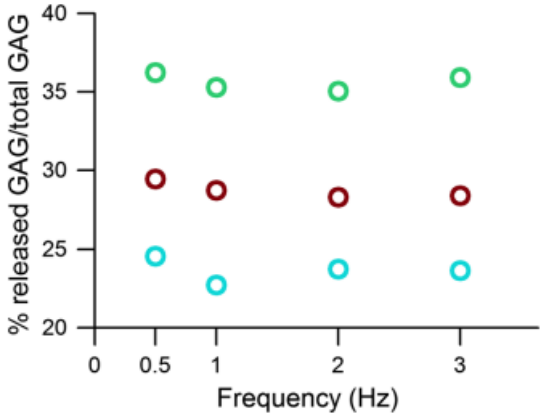
% released GAG/total GAG
40
35
30
25
20
0
0.5
1
2
3
Frequency (Hz)

**Fig. 8**

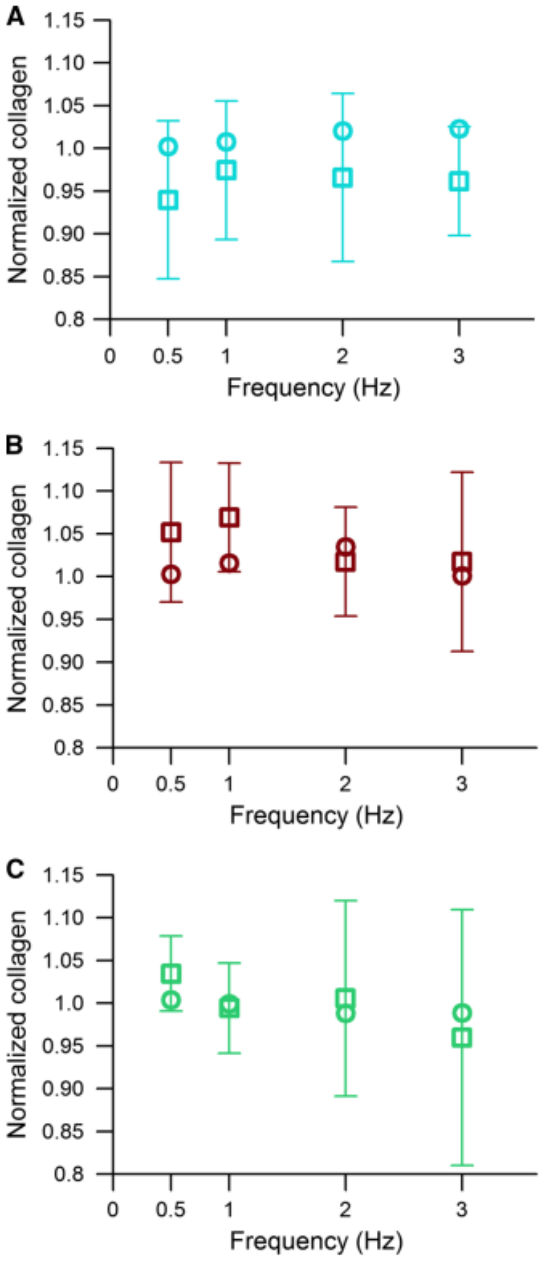
A
B
C
Normalized collagen
1.15
1.10
1.05
1.0
0.95
0.90
0.85
0.8
0
0.5
1
2
3
Frequency (Hz)

**Fig. 9**